Journal of Integrative Agriculture 2026, 25(8): 3208–3217

Available online at ScienceDirect

Journal of Integrative Agriculture



RESEARCH ARTICLE

A study on the response of planting density to 3D plant shape plasticity and population light transmittance of maize

Guangtao Wang[1, 2], Guanmin Huang[2], Weiliang Wen[2], Sheng Wu[2], Xianju Lu[2], Bo Chen[2], Xinming Ma[1#], Xinyu Guo[2#], Chunjiang Zhao[1, 2#]

[1] *College of Agronomy, Henan Agricultural University, Zhengzhou 450046, China*
[2] *Beijing Key Lab of Digital Plant/National Engineering Research Center for Information Technology in Agriculture, Beijing 100097, China*

Highlights

- During vegetative growth, maize exhibited enhanced vertical and horizontal development under increased planting density.
- At the silking stage, plants showed reduced spatial occupancy with pronounced lateral growth inhibition under increased planting density.
- The light transmission model based on support vector regression achieved reliable prediction accuracy.

Abstract

Traditional two-dimensional (2D) analyses of maize (*Zea mays* L.) plant shape plasticity and canopy transmission under varying planting densities have limitations in capturing spatial heterogeneity. This study used a three-dimensional (3D) phenotyping platform to investigate architectural plasticity across different maize varieties and planting densities. Seven novel 3D architectural parameters were developed, and 3D canopy models were constructed for light distribution simulation. At the vegetative stage 9 (V9) stage, medium planting density (67,500 plants ha^{-1}, MD) increased plant side width and convex hull volume by 7.2 and 11.4%, respectively, compared to low planting density (37,500 plants ha^{-1}, LD). High planting density (97,500 plants ha^{-1}, HD) increased the width and volume by 4.2 and 17.8%, respectively, compared with MD. Similar changes were maintained at the V13 stage. At the silking stage, the number of voxel volume plant (NVP) and projected area (PJA) decreased by 6.2 and 11.9%, respectively, under MD compared with LD, and by 4.9 and 3.6%, respectively, under HD compared with MD. Across all densities, PJA and NVP in both MC812 and JNK728 were consistently lower than in ZD958. A bottom light transmittance estimation model combining point cloud parameters with support vector regression achieved reliable predictions (R^2=0.76, RMSE=2.89%). The 3D canopy model effectively simulated population light distribution (R^2=0.83, RMSE=8.53%). NVP and PJA were identified as critical parameters affecting bottom canopy transmittance, suggesting their potential as 3D selection indices for maize density tolerance breeding. These findings provide insights into stage-specific architectural plasticity and light interception, supporting molecular design breeding of density-tolerant maize.

Keywords: maize, planting density, 3D phenotyping, light transmittance, 3D canopy model

1. Introduction

Food security depends heavily on increasing maize yield per unit area, with optimized planting density being a key strategy. Over the past 50 years, more than 50% of maize yield improvements have been attributed to increased planting density (Duvick 2005). However, higher planting densities create several challenges. These include intensified inter-plant competition, deteriorated canopy light environment, weakened stalks with higher lodging risks (Xue *et al.* 2017), and reproductive issues such as female cob degradation and increased sterility (Liu Y *et al.* 2021; Li R *et al.* 2022). Understanding plant responses to planting density, particularly architectural changes and light interception patterns, is therefore crucial for sustainable yield

Received 15 December 2024; Received in revised form 11 April 2025; Accepted 16 April 2025; Available 16 May 2025
[#]Correspondence Xinming Ma, E-mail: xinmingma@126.com; Xinyu Guo, E-mail: guoxy73@163.com; Chunjiang Zhao, E-mail: zhaocj@nercita.org.cn

© 2026 CAAS. Publishing services by Elsevier B.V. on behalf of KeAi Communications Co. Ltd. This is an open access article under the CC BY-NC-ND license (http://creativecommons.org/licenses/by-nc-nd/4.0/). Peer review under responsibility of Editorial Board of *Journal of Integrative Agriculture*.
doi: 10.1016/j.jia.2025.05.011

improvements under high-planting density systems.

Planting density significantly influences maize plant morphology as an adaptive mechanism to population competition (Li *et al.* 2021). Historical breeding trends reveal consistent selection for optimized plant architecture. Studies in Germany and France have documented annual increases in leaf erectness of 0.07% (1970–2001) and 0.11% (1950–2015), respectively (Taube *et al.* 2020; Welcker *et al.* 2022). This evolution towards more compact plant types has enhanced population-level light resource utilization. Key architectural parameters for high yield include leaf angle, leaf orientation value, and leaf area per plant (Liu *et al.* 2017). For ultra-high yields, optimal parameters include a leaf area index above 6.0 (Van Roekel and Coulter 2011) and above-ear leaf angles between 10° and 18° (Li 2000). These parameters have been validated in high-yielding varieties, with a leaf area index of 7.53 and an average above-ear leaf angle of 16.7° at the silking stage (Liu *et al.* 2017). While current research mainly relies on two-dimensional (2D) analyses, maize's complex three-dimensional (3D) structure necessitates more sophisticated spatial analysis methods.

The relationship between planting density and canopy transmittance reflects complex ecological interactions. Higher planting densities create multi-level light interception gradients through increased leaf overlap and shading (Postma *et al.* 2021). Canopy transmittance, as a 3D trait, varies with plant height, leaf angle, and leaf morphology (Xue *et al.* 2015). Various approaches have been developed to study canopy light environments, including radiative transfer modeling (Zheng *et al.* 2008), ray-tracing techniques (Bittner *et al.* 2012), and 3D radiation models for intercropping systems (Zhu *et al.* 2020). Recent advances in computer vision, such as unmanned aerial vehicle multi-angle imaging (Xiao *et al.* 2023), have opened new possibilities. However, achieving precise field-scale 3D reconstruction and light environment simulation remains challenging.

Red-green-blue (RGB) image-based 3D reconstruction offers promising solutions for plant phenotyping. Multi-view stereo (MVS) methods generate detailed point clouds from multiple image angles (Hui *et al.* 2018), improving measurement accuracy (Yang *et al.* 2024). This technology has proven effective across various crops, including wheat, sorghum, maize, and sugar beet (Pound *et al.* 2014; Xiang *et al.* 2019; Li Y *et al.* 2022; Chen *et al.* 2024). Recent developments, such as the 64-camera MVS System (Song *et al.* 2023), have further enhanced 3D modeling capabilities. However, research gaps remain in understanding dynamic 3D phenotyping changes under varying planting densities and their relationship with canopy transmittance.

To overcome the barriers to dense maize planting, an in-depth understanding of the adaptive changes in plant architecture and their impact on the population light environment from a 3D spatial perspective is essential. This study aims to develop a comprehensive understanding of maize adaptation to dense planting through three main objectives: (1) Establish a 3D phenotypic monitoring method using MVS imaging for precise plant parameter characterization; (2) investigate spatial-temporal dynamics of plant structure under different planting densities; (3) analyze relationships between 3D plant structure and canopy transmittance. The findings will advance our understanding of maize responses to dense planting and provide valuable insights for breeding programs and cultivation practices.

2. Materials and methods

2.1. Experimental design

Field experiments were conducted at the Academy of Agricultural Sciences, Gongzhuling City, Jilin Province, China (43°30′N, 124°48′E) during the 2023 and 2024 growing seasons. The experimental site is located in the Songliao Plain, which is characterized by a mid-temperate, humid continental monsoon climate. The soil type was black soil with the following properties in the plow layer (0–20 cm): pH 5.83, total organic matter 24.5 g kg^{-1}, alkaline N 138 mg kg^{-1}, available P 26.8 mg kg^{-1}, and available K 240 mg kg^{-1}.

Three maize varieties with distinct plant architectures were selected: Zhengdan 958 (ZD958, a widely cultivated hybrid with a compact architecture), MC812 (characterized by compact plant type and upright leaves), and Jingnongke 728 (JNK728, exhibiting intermediate architectural traits). These varieties with contrasting characteristics were selected to investigate plant-light relationships under density stress. The experiment followed a randomized block experiment design with three planting densities as main plots: low planting density (LD, 37,500 plants ha^{-1}), medium planting density (MD, 67,500 plants ha^{-1}), and high planting density (HD, 97,500 plants ha^{-1}). Varieties were arranged as subplots with three replicates. Each plot consisted of 12 rows with 0.6 m row spacing and 10 m length. Two seeds were initially sown per hole and then thinned to one plant at the 3-leaf stage. Fertilizer management included a basal application of N (150 kg ha^{-1}), P_2O_5 (100 kg ha^{-1}), and K_2O (120 kg ha^{-1}) before sowing, and a top-dressing of urea (150 kg ha^{-1}; N≥46%) at the vegetative stage 9 (V9). All plots received uniform fertilization and management practices for weed, disease, and pest control.

2.2. Data acquisition

Maize 3D point cloud feature extraction Three representative plants per treatment were selected for 3D point cloud acquisition at V9, vegetative stage 13 (V13), and reproductive stage 1 (R1) (Appendix A). Plants were imaged using MVS-Pheno, a low-cost phenotyping platform developed by Wu *et al.* (2020). The platform comprised a rotary motor, base, console, support arm, multiple Raspberry Pi cameras (8 MP resolution, 24 mm focal length), and a laptop computer for control. Plants were carefully transferred to pots while maintaining their field posture for imaging in an enclosed experimental room.

Camera positions were adjusted according to plant height at different growth stages, with cameras positioned at 45° to the horizontal plane to ensure 1/3 image overlap between adjacent cameras. Image acquisition was controlled wirelessly, with each camera capturing 45 RGB images (2,560×1,920 pixels) at 8° intervals during a 360° rotation, completing the process in approximately 2 min per plant (Fig. 1-A).

Point cloud reconstruction was performed using a Python-based batch pipeline and Agisoft Photoscan Professional software (Agisoft LLC, St. Petersburg, Russia). The reconstructed point clouds were processed using PlantCad-MVS software (Digital Plant Laboratory, Beijing Academy of Agriculture and Forestry Sciences, Beijing, China) for background noise removal (Fig. 1-B) and subsequent extraction of seven phenotypic parameters (Fig. 1-C; Table 1).

Canopy light distribution characteristics Canopy light distribution measurements were conducted between 10:00 a.m. and 12:00 a.m. on clear days during the V9, V13, and R1 stages. An AccuPAR LP-80 plant canopy analyzer (METER, USA) was used to measure photosynthetically active radiation (PAR) in each plot. The analyzer simultaneously recorded PAR above the canopy (PARa) and at various canopy positions (PARb) at 30 cm intervals from the ground. Three measurements were taken per plot, and light transmittance at different canopy levels was calculated according to the following formula:

Light transmittance (%)=(PARb/PARa)×100

Population construction and canopy transmittance simulation Population simulation was conducted using PlantCad software (Digital Plant Laboratory, Beijing Academy of Agricultural and Forestry Sciences). Individual plant models were generated through batch processing of point clouds, including skeleton extraction, stem and leaf segmentation, and mesh transformation. These models were used to simulate population structures by adjusting plant-row spacing according to target planting densities (Fig. 1-D). Each simulated population comprised 150 plants arranged in 10 rows and 15 columns, with plant azimuths adjusted for different planting densities. A virtual wall equivalent to 70% of plant height was constructed around the population periphery to enhance the accuracy of light distribution calculations. Light sensors were positioned at 30 cm intervals within the population center to simulate PAR capture. The PAR distribution within the 3D canopy was calculated using the Shine3DCrops software, which employs a light projection algorithm to simulate radiative interception on each canopy face (Gu *et al.* 2022). Canopy transmittance was then simulated at different canopy positions to evaluate PAR distribution patterns across planting densities (Wen *et al.* 2019, 2021).

Modelling light transmittance at the bottom of the canopy Multiple machine learning methods were applied to estimate bottom canopy transmittance, including support vector regression (SVR), random forest, partial least squares regression, and K-Nearest neighbors. The Shapley Additive exPlanations (SHAP) method was used to interpret model predictions by quantifying individual feature contributions based on Shapley values from game theory. All modeling and SHAP analyses were performed using Python-based libraries, including scikit-learn and shap.

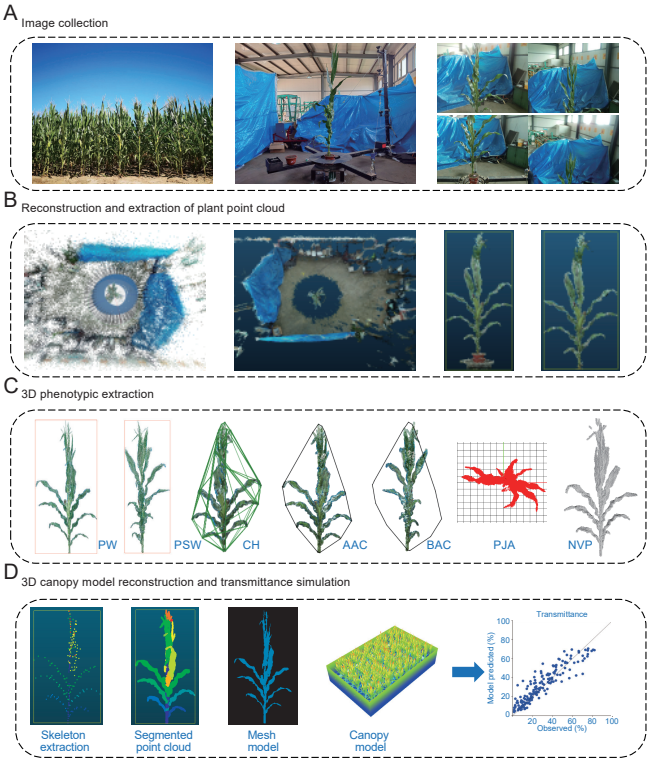


Fig. 1 Pipeline of three-dimensional (3D) canopy modeling. A, image collection with an MVS-Pheno platform. B, point cloud reconstruction and plant extraction. C, point cloud index extraction includes azimuth area convex (AAC), bottom area convex (BAC), convex hull volume (CH), projected area (PJA), plant side width (PSW), plant width (PW), and number of voxel volume plant (NVP). D, 3D canopy model reconstruction and transmittance simulation.

2.3. Statistical analyses

Data processing began with preliminary calculations in Excel 2016. Analysis of variance and LSD multiple comparison tests were performed in SPSS 27.0 (SPSS Inc., Chicago, IL, USA) to evaluate varietal differences at the $P<0.05$ level. Pearson correlation coefficients were calculated to assess parameter relationships, with significance levels set at $P<0.05$ and $P<0.01$ for significant and highly significant correlations, respectively. Visualizations were created using Origin 2024 (OriginLab, Northampton, MA, USA) and Python-based libraries. Model performance was evaluated using the coefficient of determination (R^2) and relative root mean square error (RMSE), calculated through Python's scikit-learn package. The calculation formulae are:

$$R^2=1-\frac{\sum_i (y-y')^2}{\sum_i (y-\bar{y})^2}$$

$$\text{RMSE}=\sqrt{\frac{\sum_{i=1}^{n} (y-y')^2}{n}}$$

where y and y' are the observed and model-simulated values, respectively, $\bar{y}$ is the mean of the observations, and n is the number of observations.

3. Results

3.1. Phenotypic analysis based on 3D visualization

Plant width (PW) and plant side width (PSW) Both PW and PSW in maize increased significantly throughout development (Fig. 2; Appendix B). During the V9 to V13 stages, PW and PSW increased by 16.5 and 33.3%, respectively, followed

Table 1 Overview of the phenotypic traits estimated from three-dimensional (3D) reconstructions

Symbol	Trait	Unit	Description	Reference
AAC	Azimuth area convex	cm^2	The projected convex hull area of corn plants on the azimuth plane	Wu S *et al.* (2024)
BAC	Bottom area convex	cm^2	Two-dimensional convex hull area projected by plant point cloud on the ground	Feldman *et al.* (2021)
CH	Convex hull volume	cm^3	Convex volume of plant point cloud	Xiao *et al.* (2020)
PJA	Projected area	cm^2	PJA is calculated by finding the area occupied by the projection of the voxelized point cloud onto the ground plane	Feldman *et al.* (2021)
PSW	Plant side width	cm	Plant maximum width in the side direction	Wu S *et al.* (2024)
PW	Plant width	cm	Plant maximum width in the front direction	Wu S *et al.* (2024)
NVP	Number of voxel volume plant	cm^3	Plant point cloud voxel volume, set the voxelization parameter as 1 cm×1 cm×1 cm	Klodt and Cremers (2015)

by increases of 6.8 and 12.9%, respectively, from V13 to R1. The response to planting density varied across growth stages. At V9, under MD treatment, PW and PSW increased by 3.7 and 7.2%, respectively, compared to LD, while HD treatment induced further increases of 3.7 and 4.2%, respectively, relative to MD. This pattern persisted at V13, with PSW demonstrating more pronounced changes: a 13.8% increase under MD compared to LD, and a 5.8% increase under HD compared to MD. In contrast, at R1, both parameters exhibited inverse relationships with planting density. The transition from LD to MD resulted in decreases of 3.1 and 6.4% in PW and PSW, respectively, while the shift from MD to HD led to further reductions of 2.6 and 4.5%, respectively. These responses were variety-specific yet consistent within growth stages. At V13, the MD to HD transition increased PW by 2.8, 2.5, and 1.7%, and PSW by 4.1, 3.6, and 9.6% for JNK728, MC812, and ZD958, respectively. At R1, the LD to MD transition decreased PW by 2.2, 3.0, and 4.4%, and PSW by 10.3, 5.5, and 2.3% for the respective varieties. Further density increase from MD to HD at R1 reduced PW by 4.1, 1.1, and 1.7%, and PSW by 2.5, 3.7, and 4.5% for JNK728, MC812, and ZD958, respectively. Notably, JNK728 consistently showed higher PW and PSW values than MC812 and ZD958 across all experimental conditions. Compared with JNK728, the PW of MC812 and ZD958 was lower by 13.1 and 15.3% (LD), 13.9 and 17.2% (MD), and 11.2 and 15.9% (HD), respectively. Equally, PSW was lower by 21.0 and 26.1% (LD), 16.8 and 19.6% (MD), and 17.6 and 21.0% (HD), respectively.

Convex hull volume (CH), azimuth area convex (AAC), and bottom area convex (BAC) The convex hull characteristics of maize demonstrated distinct developmental patterns across growth stages. During the vegetative growth phase (V9 to V13), CH, AAC, and BAC exhibited their most rapid increases, with increments of 120.9, 85.2, and 48.5%, respectively. The growth rate subsequently moderated during the reproductive phase (V13 to R1), with corresponding increases of 44.2, 17.8, and 27.6% (Table 2). The impact of planting density on these parameters manifested in a stage-specific manner. During vegetative growth (V9–V13), elevated planting density enhanced CH, AAC, and BAC development, with maximum effects observed at V9, followed by V13. At V9, CH, AAC, and BAC increased by 11.4, 7.5, and 12.4%, respectively, increasing planting density from LD to MD, and by 14.7, 10.8, and 3.7%, respectively, from MD to HD. At V13, increasing planting density from LD to MD resulted in increments of 7.4, 3.4, and 11.9% in CH, AAC, and BAC, respectively, while the transition from MD to HD induced further increases of 11.3, 4.5, and 2.5%. Conversely, at R1, increased planting density induced reductions in these parameters. The transition from LD to MD resulted in decreases of 6.9, 3.3, and 6.8% in CH, AAC, and BAC, respectively, while the subsequent increase from MD to HD led to further reductions of 3.6, 2.5, and 4.5%. Genotypic responses to planting density exhibited significant variation. JNK728 consistently maintained superior CH, AAC, and BAC values across all planting densities compared to MC812 and

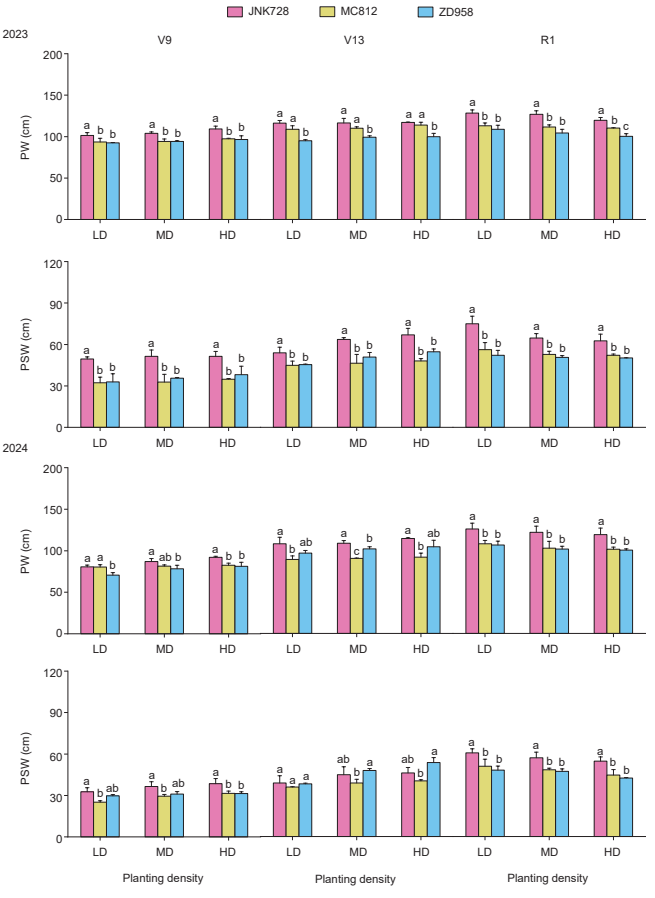


Fig. 2 Plant width (PW) and plant side width (PSW) of three varieties under different planting densities and period conditions in 2023 and 2024. LD, MD, and HD, 37,500, 67,500, and 97,500 plants ha^{-1}, respectively. V9, vegetative stage 9; V13, vegetative stage 13; R1, reproductive stage 1. JNK728, Jingnongke 728; ZD958, Zhengdan 958. Bars mean SD of three replicates. Values accompanied by different letters are different at $P<0.05$.

ZD958. At V13, when planting density increased from LD to MD, JNK728 demonstrated increases of 14.0, 5.3, and 24.2% in CH, AAC, and BAC, respectively, while ZD958 showed increases of 11.8, 8.0, and 14.5%. In contrast, MC812 exhibited a negative response, with decreases of 5.5, 3.5, and 4.7%. At R1, although all varieties displayed sensitivity to high planting densities, their response magnitudes varied considerably. Under the LD to MD transition, JNK728 exhibited the most moderate decreases (CH, 4.8%; AAC, 1.6%; BAC, 6.8%), while ZD958 demonstrated the most pronounced reductions (CH, 10.6%; AAC, 6.9%; BAC, 8.1%). Although inter-variety differences became less pronounced during the MD to HD transition, they remained statistically significant throughout the experimental period. Inter-species comparisons revealed that the CH, AAC, and BAC of JNK728 were significantly higher than those of MC812 and ZD958. Compared with JNK728, the CH of MC812 and ZD958 was 39.1 and 30.9% (LD), 40.1 and 35.1% (MD), and 38.6 and 33.2% (HD) lower than that of JNK728, respectively; AAC was lower by 20.3 and 14.1% (LD), 20.2 and 18.7% (MD), and 19.0 and 18.6% (HD), respectively; BAC was lower by 38.6 and 31.1% (LD), 37.6 and 32.0% lower (MD) and 36.7 and 30.2% (HD), respectively.

PJA and NVP PJA and NVP of maize demonstrated significant increases throughout development (Fig. 3). From V9 to V13, PJA and NVP increased by 30.6 and 121.0%, respectively, followed by further increases of 33.5 and 97.7% from V13 to R1. The response to planting density varied across developmental stages. At V9, under MD compared to LD conditions, PJA increased by 4.1% while NVP decreased by 4.8%. Similarly, the transition from MD to HD conditions resulted in a 3.7% increase in PJA and a 2.9% decrease in NVP. This pattern persisted through V13, albeit with greater changes than in V9. Conversely, at R1, both parameters exhibited significant decreases with increasing planting density. The transition from LD to MD conditions resulted in reductions of 6.2 and 11.9% in PJA and NVP, respectively, while further density increase from MD to HD led to additional decreases of 4.9 and 3.6%. While the directional responses to planting density remained consistent across varieties at different growth stages, the magnitude of these responses showed genotypic variation. At V9, when planting density increased from MD to HD, PJA increased by 1.7, 4.8, and 4.8%, while NVP decreased by 4.3, 2.2, and 2.2% for JNK728, MC812, and ZD958, respectively. At R1, both parameters demonstrated progressive decreases with increasing planting density. Under the MD to HD transition, PJA decreased by 5.2, 4.7, and 4.7%, while NVP decreased by 2.6, 7.3, and 1.4% for JNK728, MC812, and ZD958, respectively. Notably, ZD958 maintained consistently higher

Table 2 Effects of growth stage and planting density on point cloud parameters[1)]

Year	Genotype[2)]	Planting density (plants ha^{-1})	V9[3)]			V13[3)]			R1[3)]		
			CH (×10^4 cm^3)	AAC (cm^2)	BAC (cm^2)	CH (×10^4 cm^3)	AAC (cm^2)	BAC (cm^2)	CH (×10^4 cm^3)	AAC (cm^2)	BAC (cm^2)
2023	JNK728	37,500	10.3 a	6,467.0 a	1,846.0 a	33.0 a	16,156.7 a	3,056.4 a	68.8 a	21,719.9 a	5,158.8 a
	MC812		8.1 b	6,326.6 a	1,421.2 a	25.4 b	13,428.2 b	2,535.9 b	41.0 c	16,016.1 b	3,662.1 c
	ZD958		8.6 b	5,521.6 b	1,597.0 a	31.7 a	15,104.7 a	2,931.4 ab	50.8 b	19,711.5 a	4,389.1 b
	JNK728	67,500	11.5 a	6,606.7 a	2,208.3 a	38.5 a	17,775.0 a	3,613.8 a	65.6 a	21,073.4 a	4,838.7 a
	MC812		9.5 b	6,404.3 a	1,634.4 a	23.2 b	12,557.9 b	2,332.1 b	39.6 b	15,935.0 c	3,528.3 b
	ZD958		9.5 b	6,507.6 a	1,661.7 a	37.6 a	16,282.0 a	3,560.1 a	45.4 b	17,810.1 b	4,015.5 b
	JNK728	97,500	16.9 a	9,496.1 a	2,457.0 a	47.9 a	20,646.2 a	3,848.2 a	61.9 a	20,738.3 a	4,636.8 a
	MC812		9.9 b	6,498.4 b	1,700.1 b	22.7 b	12,075.9 c	2,151.7 b	38.8 b	1,5692.6 c	3,391.1 b
	ZD958		10.6 b	6,775.3 b	1,793.6 b	44.1 a	17,549.4 b	3,767.5 a	44.9 b	17,620.7 b	3,861.3 b
2024	JNK728	37,500	28.2 a	10,619.1 a	3,415.9 a	39.7 a	18,209.0 a	3,712.4 a	75.6 a	22,061.8 a	6,905.9 a
	MC812		13.9 b	8,207.2 b	1,965.8 b	34.3 b	15,744.0 b	3,456.9 a	46.9 b	18,884.6 b	3,739.7 b
	ZD958		16.9 b	9,756.4 a	2,034.1 b	35.0 b	13,652.5 b	3,121.9 a	49.0 b	17,884.0 b	3,926.0 b
	JNK728	67,500	29.3 a	11,461.2 a	3,766.8 a	44.4 a	18,419.4 a	4,795.9 a	71.9 a	21,993.5 a	6,403.9 a
	MC812		15.4 b	9,259.1 b	2,008.4 b	33.2 b	15,588.3 b	3,381.4 b	42.8 b	18,412.6 b	3,488.0 b
	ZD958		20.6 b	10,178.9 ab	2,518.0 b	37.0 b	14,774.4 b	3,373.1 b	43.8 b	17,204.7 b	3,626.2 b
	JNK728	97,500	32.6 a	13,133.0 a	3,862.4 a	49.8 a	18,726.2 a	5,129.5 a	68.7 a	21,052.6 a	5,979.4 a
	MC812		19.9 b	10,860.3 b	2,514.0 b	31.6 b	15,296.3 b	3,211.4 b	41.4 b	18,169.9 b	3,328.5 b
	ZD958		23.0 b	11,054.4 b	2,966.3 b	42.0 a	15,354.8 b	3,465.9 b	42.3 b	16,376.6 c	3,550.3 b
ANOVA											
Year (Y)			405.3***	786.3***	116.4***	18.1***	2.8 NS	67.0***	4.3*	5.8*	12.4**
Genotype (G)			81.6***	59.5***	50.7***	56.1***	78.3***	73.8***	144.7***	101.6***	144.1***
Planting density (PD)			20.5***	63.9***	10.4***	12.8***	6.4**	12.6***	5.7**	5.9**	7.2**
Y×G			25.1***	7.6**	9.7***	6.2**	22.3***	22.3***	3.3*	17.6***	29.4***
Y×PD			1.0 NS	2.1 NS	0.9 NS	1.0 NS	1.9 NS	0.1 NS	0.1 NS	0.3 NS	0.1 NS
G×PD			0.6 NS	6.3***	0.2 NS	6.4***	5.0**	9.5***	0.2 NS	0.8 NS	0.4 NS
Y×G×PD			1.4 NS	5.3**	0.9 NS	0.3 NS	2.2 NS	1.6 NS	0.1 NS	0.3 NS	0.2 NS

[1)] V9, vegetative stage 9; V13, vegetative stage 13; R1, reproductive stage 1.
[2)] JNK728, Jingnongke 728; ZD958, Zhengdan 958.
[3)] CH, convex hull volume; AAC, azimuth area convex; BAC, bottom area convex.
Values represent the means of three replicates. Values within each column followed by the same letter are not different at P<0.05. *, ** and *** indicate significances at the 0.05, 0.01 and 0.001 probalility levels, respectively; NS, no significance.

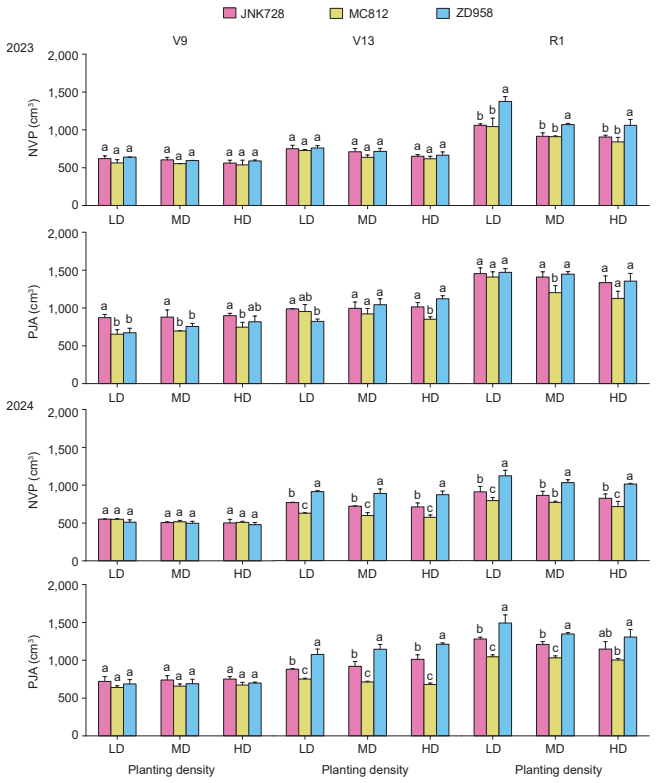


Fig. 3 Number of voxel volume plant (NVP) and projected area (PJA) of three varieties under different planting densities and period conditions in 2023 and 2024. LD, MD, and HD, 37,500, 67,500, and 97,500 plants ha^{-1}, respectively. V9, vegetative stage 9; V13, vegetative stage 13; R1, reproductive stage 1. JNK728, Jingnongke 728; ZD958, Zhengdan 958. Bars mean SD of three replicates. Values accompanied by different letters are different at P<0.05.

NVP values across all planting densities compared to JNK728 and MC812, while simultaneously exhibiting relatively high PJA values. Compared with ZD958, the PJA of MC812 and JNK728 was lower by 17.2 and 7.6% (LD), 20.0 and 6.2% (MD), 20.0 and 6.7% (HD), respectively. Similarly, their NVP was lower by 26.5 and 21.1% (LD), 20.0 and 15.4% (MD), 24.8 and 16.4% (HD), respectively.

3.2. Canopy transmittance simulation based on canopy model

Canopy transmittance Canopy transmittance exhibited significant progressive reductions across developmental stages (Fig. 4; Appendix C). The bottom canopy transmittance diminished markedly, with a 44.6% reduction from V9 to V13, followed by a 38.5% decrease from V13 to R1. Elevated planting density intensified the reduction in canopy transmittance throughout all growth stages, with the most substantial effects manifesting at R1. Under MD, bottom canopy transmittance decreased by 48.7% relative to LD conditions, while HD conditions induced a further 61.9% reduction compared to MD. Although similar patterns were observed during the V9 and V13 stages, the magnitude of reduction was less pronounced. Distinct genotypic variations in canopy transmittance were observed, consistently following the pattern MC812>JNK728>ZD958 across all growth stages and density treatments. This hierarchical pattern was particularly evident in ear layer transmittance at R1, where MC812 demonstrated 32.5 and 71.9% higher bottom transmittance than JNK728 and ZD958, respectively (Appendix D). The response to increased planting density exhibited genotype-specific variations. The transition from LD to MD conditions resulted in bottom canopy transmittance reductions of 44.9, 49.9, and 51.6% for JNK728, MC812, and ZD958, respectively. Subsequent density increases from MD to HD led to further reductions of 64.8, 57.5, and 65.7%, respectively.

Canopy modeling and canopy light distribution simulation 3D canopy architectures of the maize varieties were digitally reconstructed using PlantCad software, based on acquired 3D point cloud data. The architectural representations at R1 under varying planting densities are shown in Appendix E. Each virtual population comprised 150 plants configured in a 10×15 matrix arrangement, maintaining a consistent row spacing of 0.6 m. Simulation analyses revealed that elevated planting density resulted in diminished inter-plant spacing and reduced canopy gaps, consequently yielding a more compact population footprint while maintaining plant quantity. Temporal simulations conducted under MD (Fig. 5-A) demonstrated progressive decreases in canopy transmittance corresponding to increased plant height throughout developmental stages. PAR measurements at distinct canopy positions were obtained by positioning a virtual light sensor at the central point of the canopy model,

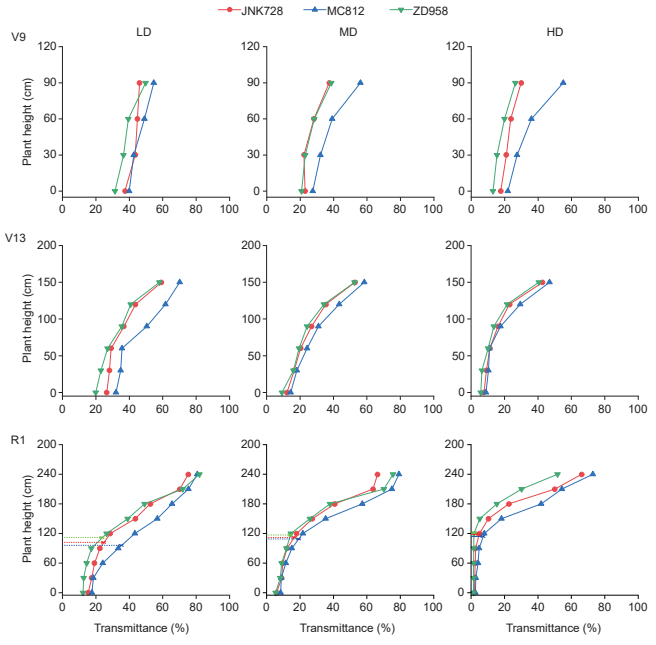


Fig. 4 Canopy transmittance of three varieties under different planting densities and period conditions in 2023. Each symbol represents the mean of three replicates. The dashed line represents the ear layer. LD, MD, and HD, 37,500, 67,500, and 97,500 plants ha^{-1}, respectively. V9, vegetative stage 9; V13, vegetative stage 13; R1, reproductive stage 1. JNK728, Jingnongke 728; ZD958, Zhengdan 958.

utilizing Shine3DCrops software. Comparative analysis between field measurements and model simulations (Fig. 5-B) validated the model's capacity to accurately characterize canopy light distribution patterns during the reproductive period (R^2=0.83, RMSE=8.53%). Stage-specific validation analyses revealed optimal simulation accuracy at V13 (R^2=0.88, RMSE=5.76%), followed by R1 (R^2=0.84, RMSE=10.16%), while the V9 stage exhibited comparatively lower precision (R^2=0.50, RMSE=7.95%). Further scatter plot analysis indicated a tendency toward model overestimation at both V9 and V13.

3.3. Identification of sensitive parameters of maize canopy transmittance

A predictive model for maize canopy transmittance was developed utilizing point cloud parameters, accompanied by the identification of key sensitivity indicators. Comparative assessment of four machine learning algorithms (Fig. 6-A–D) demonstrated superior predictive performance of the SVR model (R^2=0.76, RMSE=2.89%), substantially exceeding the capabilities of Random Forest (R^2=0.56, RMSE=5.41%), Partial Least Squares Regression (R^2=0.55, RMSE=4.95%), and K-Nearest Neighbors (R^2=0.39, RMSE=6.73%). Nevertheless, the model exhibited a consistent tendency toward overestimation in its predictions. Feature importance analysis elucidated the relative contributions of distinct point cloud parameters to model predictions. NVP and PJA emerged as the predominant metrics influencing canopy transmittance (Fig. 6-E). Spatiotemporal dynamic analysis (Appendix F) revealed significant interactive effects between developmental stages and planting density on parameter sensitivity. At V9, no significant correlations were detected between any parameters and canopy transmittance. The V13 stage exhibited a significant negative correlation between PJA and transmittance under both MD and HD, while NVP demonstrated significant correlation exclusively under MD. At R1, both PJA and NVP displayed consistent, significant negative correlations with transmittance across all planting density treatments.

4. Discussion

4.1. Effects of different growth periods and planting densities on plant type and canopy light distribution

Maize exhibited distinct morphological adaptations across three growth phases in response to planting density. During the pre-V9 stage, significant increases in PW and PSW indicated early adaptation to density stress through enhanced spatial occupancy (Fig. 2; Table 2). This early response aligns with Shi *et al.* (2024), who reported density sensitivity at the 6-leaf stage through stalk diameter and leaf angle adjustments. The V9–V13 phase was characterized by continued increases in plant parameters with rising density, as plants showed both lateral and longitudinal expansion to maximize space utilization and minimize mutual shading. These morphological changes are consistent with previous studies showing increased plant height and leaf area under high-density conditions (Markham and Stoltenberg 2010; Wang *et al.* 2020). During V13–R1, plant parameters decreased with increasing density, indicating reduced spatial occupancy. Plants exhibited predominantly vertical adjustments, with leaves growing parallel to neighbors and perpendicular to row direction (Wu Y *et al.* 2024). This architectural modification improved light interception efficiency, supporting previous findings by Maddonni *et al.*

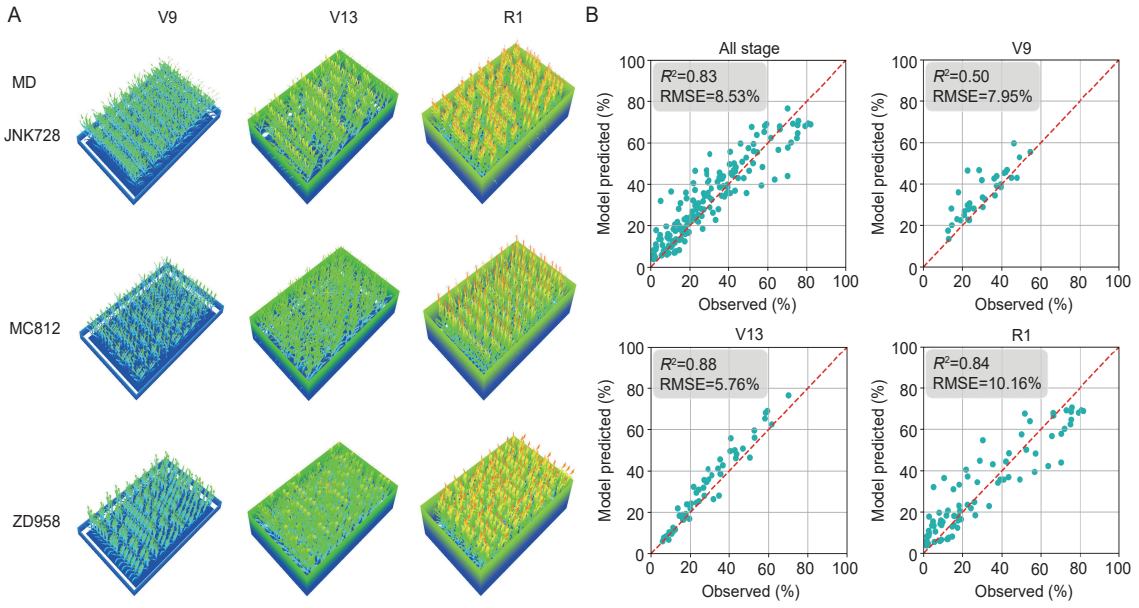


Fig. 5 Canopy light distribution simulation based on the three-dimensional (3D) canopy model. A, an example of the 3D canopy model of different varieties under the MD (67,500 plants ha^{-1}) condition at different growth stages. B, comparison results of canopy transmittance extracted from the 3D canopy model with observed values. V9, vegetative stage 9; V13, vegetative stage 13; R1, reproductive stage 1. JNK728, Jingnongke 728; ZD958, Zhengdan 958.

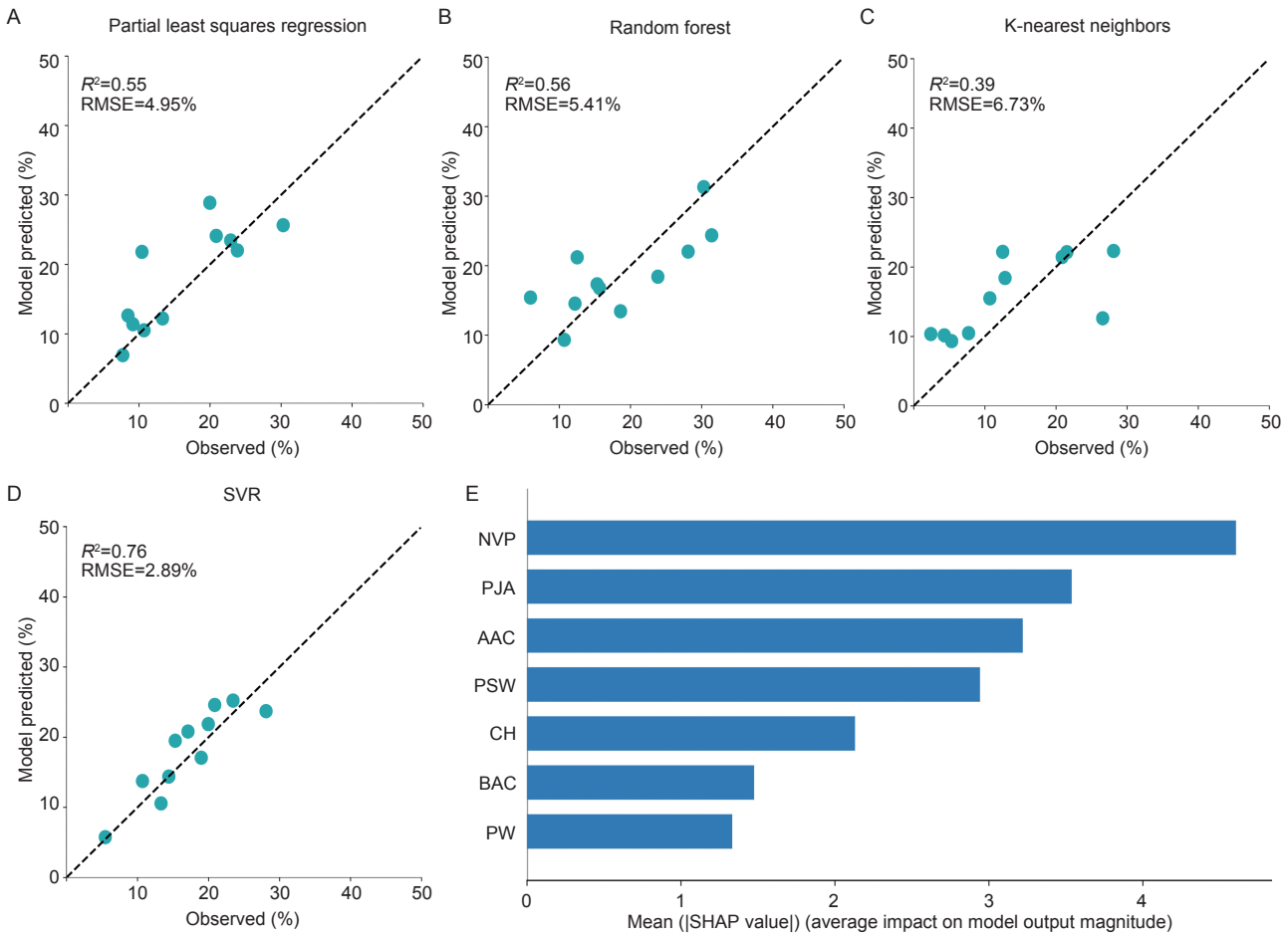


Fig. 6 Simulation of canopy base transmittance based on three-dimensional (3D) point cloud parameters. A–D, different modeling approaches. E, feature importance analysis based on the Shapley Additive exPlanations (SHAP). SVR, support vector regression; NVP, number of voxel volume plant; PJA, projected area; AAC, azimuth area convex; PSW, plant side width; CH, convex hull volume; BAC, bottom area convex; PW, plant width.

(2001) and Zhou *et al.* (2024).

In addition, at R1, under LD conditions, plants had a larger growth space (Table 2), which led to a more dispersed distribution of leaf azimuth angle and improved population light interception by maximizing plant morphology (Wu Y *et al.* 2024). As density increased, the decline amplitudes of indices in different dimensions decreased significantly (Figs. 2 and 3; Table 2), and the ability of plants to adjust space occupancy gradually weakened. Gou *et al.* (2017) found that with the increase of density, the increase of leaf direction value decreased, which slowed down the morphological convergence of plants. Genotypic differences in the adaptation of varieties to dense planting environments are influenced by a combination of genetic factors and the growing environment (Li *et al.* 2021). JNK728 had higher PW and PSW across different planting densities and growth stages, which enabled it to maintain higher CH and plant space occupancy among the three varieties (Fig. 2; Table 2). In addition, NVP was closely related to plant leaf area (Klodt and Cremers 2015). With increasing density, the leaf area decreased, resulting in a decrease of NVP at different growth stages (Fig. 3). ZD958 maintained higher NVP across different planting densities, which greatly affected its canopy structure and further impacted light energy utilization.

Canopy transmittance decreased significantly with increasing density, particularly at R1 (Fig. 4). Sensitive parameter analysis revealed NVP and PJA as primary contributors to light transmittance variations (Fig. 6-E). These findings suggest that high planting density compromises internal light distribution, potentially affecting yield through reduced lower canopy photosynthesis, consistent with Liu G *et al.* (2021) and (Chen *et al.* 2019). The deterioration of canopy light environment under high density was particularly evident in lower canopy layers, which could significantly impact overall photosynthetic efficiency and yield potential (Yan *et al.* 2024). Parameter sensitivity varied across growth stages, highlighting the need for stage-specific management strategies. Early growth stages benefit from horizontal leaf distribution optimization, while later stages require vertical adjustments for efficient light capture under dense planting.

4.2. Factors affecting canopy transmittance in a maize canopy

The three tested varieties showed distinct density responses,

reflecting genetic variation in density tolerance (Ci *et al.* 2012; Ma *et al.* 2022). JNK728 maintained a higher plant space percentage and canopy transmittance than ZD958 at high densities. MC812's compact architecture, characterized by smaller NVP and PJA (Figs. 3 and 4; Appendix C), resulted in superior canopy transmittance, demonstrating enhanced density tolerance. These findings support previous research emphasizing the role of compact architecture in optimizing light distribution (Vazin *et al.* 2010; Tian *et al.* 2019; Li *et al.* 2021). The observed genotypic differences provide valuable phenotypic indices for screening density-tolerant varieties and guidance for breeding programs aimed at improving density adaptation.

This study employed MVS imaging to acquire 3D phenotyping (Fig. 1-C), enabling comprehensive analysis of spatial structural characteristics. This approach, combined with SVR modeling for light transmittance prediction (Fig. 6-D), provides novel insights into crop phenotype-light environment interactions, complementing previous research by Zhu *et al.* (2020) and Xiao *et al.* (2023). The developed light environment simulation method showed improved efficiency compared to traditional approaches (Gu *et al.* 2022), although factors such as leaf optical properties and mutual shading require further investigation (Gitelson *et al.* 2019; Chang *et al.* 2022).

4.3. Limitations and future work

While this study provides valuable insights, several limitations warrant attention in future research. The study included only three maize varieties and specific environmental conditions, potentially limiting the generalizability of the findings. Additionally, the simulation accuracy at V9 requires improvement, and interactions with nitrogen fertilization were not examined (Ma *et al.* 2022). Future studies should expand genetic diversity sampling, incorporate varied environmental conditions, optimize model accuracy across growth stages, and enhance prediction reliability through advanced modeling techniques.

This pioneering application of multi-view 3D reconstruction in maize population analysis represents a significant advancement in crop phenomics. The study revealed key mechanisms of architectural adaptation to planting density and identified specific traits (NVP and PJA) for breeding selection. Despite current limitations, this integrated approach to 3D phenotyping and light environment simulation provides valuable tools for precision agriculture and breeding programs. Future research addressing the identified constraints will further enhance our understanding of density-dependent responses and support sustainable high-density cultivation practices.

5. Conclusion

This study developed an integrated approach combining 3D point cloud analysis with canopy light distribution to investigate plant–light interactions in maize. Plant spatial occupation reached the maximum at the silking stage, with enhanced vertical and horizontal development during vegetative growth and reduced spatial occupancy at the silking stage under high density, demonstrating architectural plasticity across varieties. The established models effectively quantified the relationships between plant architecture and light distribution, revealing that spatial structure optimization improved canopy light interception efficiency. These findings provide novel insights into maize architectural optimization for high-density planting systems, offering valuable tools for understanding plant–environment interactions and supporting both cultivation research and precision breeding applications.

Acknowledgements

The work was funded by the Construction of Collaborative Innovation Center of Beijing Academy of Agriculture and Forestry Sciences, China (KJCX20240406), the State Key Program of National Natural Science Foundation of China (32330075), and the China Postdoctoral Science Foundation (2023M730314).

Declaration of competing interest

The authors declare that they have no conflict of interest.

Declaration of generative AI and AI-assisted technologies in the writing process

The authors declare that they did not use AI in the preparation and writing of this manuscript.

Appendices associated with this paper are available at https://doi.org/10.1016/j.jia.2025.05.011

References

Bittner S, Gayler S, Biernath C, Winkler J B, Seifert S, Pretzsch H, Priesack E. 2012. Evaluation of a ray-tracing canopy light model based on terrestrial laser scans. *Canadian Journal of Remote Sensing*, **38**, 619–628.

Chang T G, Shi Z, Zhao H, Song Q, He Z, Van Rie J, Den Boer B, Galle A, Zhu X G. 2022. 3dCAP-Wheat: An open-source comprehensive computational framework precisely quantifies wheat foliar, nonfoliar, and canopy photosynthesis. *Plant Phenomics*, **2022**, 28–46.

Chen H, Zhang M, Xiao S, Wang Q, Cai Z, Dong Q, Feng P, Shao K, Ma Y. 2024. Quantitative analysis and planting optimization of multi-genotype sugar beet plant types based on 3D plant architecture. *Computers and Electronics in Agriculture*, **225**, 109231.

Chen T W, Cabrera-Bosquet L, Alvarez Prado S, Perez R, Artzet S, Pradal C, Coupel-Ledru A, Fournier C, Tardieu F. 2019. Genetic and environmental dissection of biomass accumulation in multi-genotype maize canopies. *Journal of Experimental Botany*, **70**, 2523–2534.

Ci X, Li M, Xu J, Lu Z, Bai P, Ru G, Liang X, Zhang D, Li X, Bai L, Xie C, Hao Z, Zhang S, Dong S. 2012. Trends of grain yield and plant traits in Chinese maize cultivars from the 1950s to the 2000s. *Euphytica*, **185**, 395–406.

Duvick D N. 2005. The contribution of breeding to yield advances in maize (*Zea mays* L.). *Advances in Agronomy*, **86**, 83–145.

Feldman A, Wang H, Fukano Y, Kato Y, Ninomiya S, Guo W. 2021. EasyDCP: An affordable, high-throughput tool to measure plant phenotypic traits in 3D. *Methods in Ecology and Evolution*, **12**, 1679–1686.

Gitelson A, Viña A, Solovchenko A, Arkebauer T, Inoue Y. 2019. Derivation of canopy light absorption coefficient from reflectance spectra. *Remote Sensing of Environment*, **231**, 111276.

Gou L, Xue J, Qi B, Ma B, Zhang W. 2017. Morphological variation of maize cultivars in response to elevated plant densities. *Agronomy Journal*, **109**, 1443–1453.

Gu S, Wen W, Xu T, Lu X, Yu Z, Guo X, Zhao C. 2022. Use of 3D modeling to refine predictions of canopy light utilization: A comparative study on canopy photosynthesis models with different dimensions. *Frontiers in Plant Science*, **13**, 735981.

Hui F, Zhu J, Hu P, Meng L, Zhu B, Guo Y, Li B, Ma Y. 2018. Image-based dynamic quantification and high-accuracy 3D evaluation

of canopy structure of plant populations. *Annals of Botany*, **121**, 1079–1088.
Klodt M, Cremers D. 2015. High-resolution plant shape measurements from multi-view stereo reconstruction. In: Agapito L, Bronstein M M, Rother C, eds., *Computer Vision-ECCV 2014 Workshops*. Lecture Notes in Computer Science, Springer International Publishing, Cham. pp. 174–184.
Li D H. 2000. Retrospect and prospect in breeding of compact corn. *Crops*, **5**, 1–5. (in Chinese)
Li R, Hu D, Ren H, Yang Q, Dong S, Zhang J, Zhao B, Liu P. 2022. How delaying post-silking senescence in lower leaves of maize plants increases carbon and nitrogen accumulation and grain yield. *The Crop Journal*, **10**, 853–863.
Li R, Zhang G, Liu G, Wang K, Xie R, Hou P, Ming B, Wang Z, Li S. 2021. Improving the yield potential in maize by constructing the ideal plant type and optimizing the maize canopy structure. *Food and Energy Security*, **10**, e312.
Li Y, Liu J, Zhang B, Wang Y, Yao J, Zhang X, Fan B, Li X, Hai Y, Fan X. 2022. Three-dimensional reconstruction and phenotype measurement of maize seedlings based on multi-view image sequences. *Frontiers in Plant Science*, **13**, 974339.
Liu G, Hou P, Xie R, Ming B, Wang K, Xu W, Liu W, Yang Y, Li S. 2017. Canopy characteristics of high-yield maize with yield potential of 22.5 Mg ha^{-1}. *Field Crops Research*, **213**, 221–230.
Liu G, Liu W, Hou P, Ming B, Yang Y, Guo X, Xie R, Wang K, Li S. 2021. Reducing maize yield gap by matching plant density and solar radiation. *Journal of Integrative Agriculture*, **20**, 363–370.
Liu Y, Jafari F, Wang H. 2021. Integration of light and hormone signaling pathways in the regulation of plant shade avoidance syndrome. *aBIOTECH*, **2**, 131–145.
Ma D, Xie R, Yu X, Li S, Gao J. 2022. Historical trends in maize morphology from the 1950s to the 2010s in China. *Journal of Integrative Agriculture*, **21**, 2159–2167.
Maddonni G A, Chelle M, Drouet J L, Andrieu B. 2001. Light interception of contrasting azimuth canopies under square and rectangular plant spatial distributions: Simulations and crop measurements. *Field Crops Research*, **70**, 1–13.
Markham M Y, Stoltenberg D E. 2010. Corn morphology, mass, and grain yield as affected by early-season red:far-red light environments. *Crop Science*, **50**, 273–280.
Postma J A, Hecht V L, Hikosaka K, Nord E A, Pons T L, Poorter H. 2021. Dividing the pie: A quantitative review on plant density responses. *Plant, Cell & Environment*, **44**, 1072–1094.
Pound M P, French A P, Murchie E H, Pridmore T P. 2014. Automated recovery of three-dimensional models of plant shoots from multiple color images. *Plant Physiology*, **166**, 1688–1698.
Van Roekel R J, Coulter J A. 2011. Agronomic responses of corn to planting date and plant density. *Agronomy Journal*, **103**, 1414–1422.
Shi Q, Xia Y, Wang Q, Lv K, Yang H, Cui L, Sun Y, Wang X, Tao Q, Song X, Xu D, Xu W, Wang X, Wang X, Kong F, Zhang H, Li B, Li P, Wang H, Li G. 2024. Phytochrome B interacts with LIGULELESS1 to control plant architecture and density tolerance in maize. *Molecular Plant*, **17**, 1255–1271.
Song Q, Liu F, Bu H, Zhu X G. 2023. Quantifying contributions of different factors to canopy photosynthesis in 2 maize varieties: Development of a novel 3D canopy modeling pipeline. *Plant Phenomics*, **5**, 0075.
Taube F, Vogeler I, Kluß C, Herrmann A, Hasler M, Rath J, Loges R, Malisch C S. 2020. Yield progress in forage maize in NW Europe — Breeding progress or climate change effects? *Frontiers in Plant Science*, **11**, 1214.
Tian J, Wang C, Xia J, Wu L, Xu G, Wu W, Li D, Qin W, Han X, Chen Q, Jin W, Tian F. 2019. Teosinte ligule allele narrows plant architecture and enhances high-density maize yields. *Science*, **365**, 658–664.
Vazin F, Hassanzadeh M, Madani A, Nassiri-Mahallati M, Nasri M. 2010. Modeling light interception and distribution in mixed canopy of common cocklebur (*Xanthium stramarium* L.) in competition with corn. *Planta Daninha*, **28**, 455–462.
Wang B, Lin Z, Li X, Zhao Y, Zhao B, Wu G, Ma X, Wang H, Xie Y, Li Q, Song G, Kong D, Zheng Z, Wei H, Shen R, Wu H, Chen C, Meng Z, Wang T, Li Y, *et al.* 2020. Genome-wide selection and genetic improvement during modern maize breeding. *Nature Genetics*, **52**, 565–571.
Welcker C, Spencer N A, Turc O, Granato I, Chapuis R, Madur D, Beauchene K, Gouesnard B, Draye X, Palaffre C, Lorgeou J, Melkior S, Guillaume C, Presterl T, Murigneux A, Wisser R J, Millet E J, Van Eeuwijk F, Charcosset A, Tardieu F. 2022. Physiological adaptive traits are a potential allele reservoir for maize genetic progress under challenging conditions. *Nature Communications*, **13**, 3225.
Wen W, Guo X, Li B, Wang C, Wang Y, Yu Z, Wu S, Fan J, Gu S, Lu X. 2019. Estimating canopy gap fraction and diffuse light interception in 3D maize canopy using hierarchical hemispheres. *Agricultural and Forest Meteorology*, **276–277**, 107594.
Wen W, Wang Y, Wu S, Liu K, Gu S, Guo X. 2021. 3D phytomer-based geometric modelling method for plants — The case of maize. *AoB Plants*, **13**, plab055.
Wu S, Wen W, Wang Y, Fan J, Wang C, Gou W, Guo X. 2020. MVS-Pheno: A portable and low-cost phenotyping platform for maize shoots using multiview stereo 3D reconstruction. *Plant Phenomics*, **2020**, 1848437.
Wu S, Zhang Y, Zhao Y, Wen W, Wang C, Lu X, Guo M, Guo X, Zhao J, Zhao C. 2024. Using high-throughput phenotyping platform MVS-Pheno to decipher the genetic architecture of plant spatial geometric 3D phenotypes for maize. *Computers and Electronics in Agriculture*, **225**, 109259.
Wu Y, Wen W, Gu S, Huang G, Wang C, Lu X, Xiao P, Guo X, Huang L. 2024. Three-dimensional modeling of maize canopies based on computational intelligence. *Plant Phenomics*, **6**, 0160.
Xiang L, Bao Y, Tang L, Ortiz D, Salas-Fernandez M G. 2019. Automated morphological traits extraction for sorghum plants via 3D point cloud data analysis. *Computers and Electronics in Agriculture*, **162**, 951–961.
Xiao S, Chai H, Shao K, Shen M, Wang Q, Wang R, Sui Y, Ma Y. 2020. Image-based dynamic quantification of aboveground structure of sugar beet in field. *Remote Sensing*, **12**, 269.
Xiao S, Fei S, Li Q, Zhang B, Chen H, Xu D, Cai Z, Bi K, Guo Y, Li B, Chen Z, Ma Y. 2023. The importance of using realistic 3D canopy models to calculate light interception in the field. *Plant Phenomics*, **5**, 0082.
Xue H, Han Y, Li Y, Wang G, Feng L, Fan Z, Du W, Beifang Yang, Cao C, Mao S. 2015. Spatial distribution of light interception by different plant population densities and its relationship with yield. *Field Crops Research*, **184**, 17–27.
Xue J, Xie R, Zhang W, Wang K, Hou P, Ming B, Gou L, Li S. 2017. Research progress on reduced lodging of high-yield and -density maize. *Journal of Integrative Agriculture*, **16**, 2717–2725.
Yan Y, Duan F, Li X, Zhao R, Hou P, Zhao M, Li S, Wang Y, Dai T, Zhou W. 2024. Photosynthetic capacity and assimilate transport of the lower canopy influence maize yield under high planting density. *Plant Physiology*, **195**, 2652–2667.
Yang D, Yang H, Liu D, Wang X. 2024. Research on automatic 3D reconstruction of plant phenotype based on Multi-View images. *Computers and Electronics in Agriculture*, **220**, 108866.
Zheng B, Shi L, Ma Y, Deng Q, Li B, Guo Y. 2008. Comparison of architecture among different cultivars of hybrid rice using a spatial light model based on 3-D digitising. *Functional Plant Biology*, **35**, 900.
Zhou Y, Kusmec A, Schnable P S. 2024. Genetic regulation of self-organizing azimuthal canopy orientations and their impacts on light interception in maize. *The Plant Cell*, **36**, 1600–1621.
Zhu B, Liu F, Xie Z, Guo Y, Li B, Ma Y. 2020. Quantification of light interception within image-based 3-D reconstruction of sole and intercropped canopies over the entire growth season. *Annals of Botany*, **126**, 701–712.

Executive Editor-in-Chief Shaokun Li
Managing Editor Ning Wang